Electronic Supplementary Material (ESI) for Journal of Materials Chemistry C.

Supporting Information for "Charge carrier concentration dependence of ultrafast plasmonic relaxation in conducting metal oxide nanocrystals"

Robert W. Johns,[1,2*] Michelle A. Blemker,[3*] Michael S. Azzaro,[3] Sungyeon Heo,[2] Evan L. Runnerstrom,[2,4] Delia J. Milliron,[2] & Sean T. Roberts[3‡]

1. Department of Chemistry, University of California, Berkeley, Berkeley, California 94720, USA.

2. McKetta Department of Chemical Engineering, The University of Texas at Austin, 200 East Dean Keeton Street, Austin, Texas 78712, USA.

3. Department of Chemistry, The University of Texas at Austin, Austin, Texas 78712-1224, United States

4. Department of Materials Science and Engineering, The University of California, Berkeley, Berkeley, California 94720, United States

[*] These two authors contributed equally to this manuscript.
[‡] Author to whom correspondence should be sent: roberts@cm.utexas.edu

STEM Images of Metal Oxide Nanocrystals

Figure S1 displays STEM images of $Sn:In_2O_3$ and cubic WO_{3-x} nanocrystals (NCs) used for steady-state and transient absorption (TA) measurements. These images were measured for samples dropcast on a holey carbon TEM grid and measured using a Hitachi S5500 STEM.

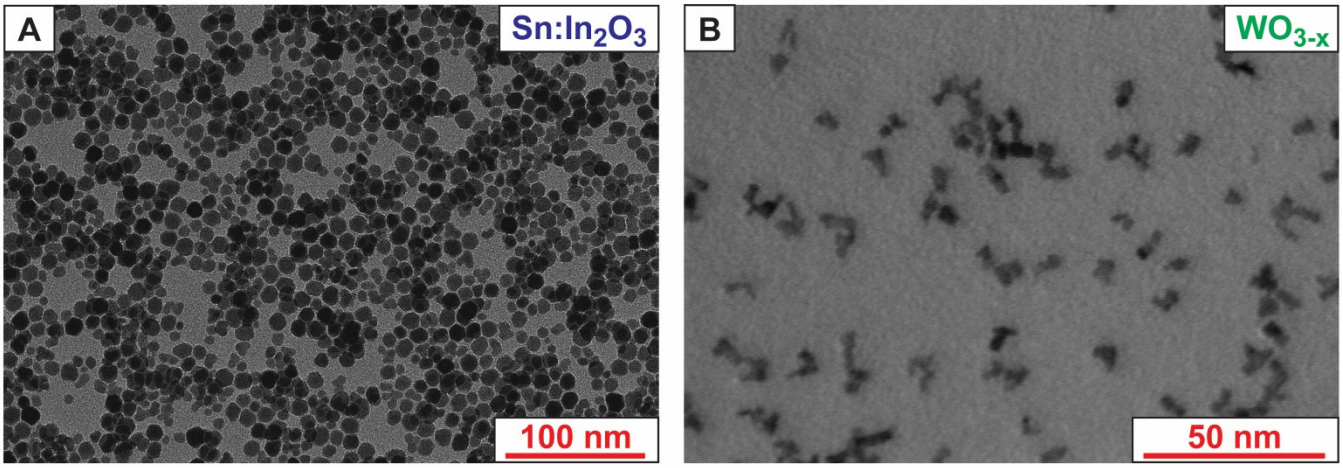

Figure S1: STEM images of bixbyite $Sn:In_2O_3$ (a) and cubic WO_{3-x} (b) used for Drude fitting and TA measurements.

Metal Oxide Nanocrystal Steady-state Absorption Spectra

Figure S2A displays steady-state absorption spectra of metal oxide NC suspensions used for TA measurements shown in Figure 4 of the main text. Spectra of $Sn:In_2O_3$ NCs were measured in TCE while WO_{3-x} NCs were measured in hexane and both reported spectra we recorded using a 0.1 cm pathlength cuvette. It is important to note WO_{3-x}'s broad absorption lineshape, which influences the amount of material needed to reach a comparable OD to samples of higher carrier concentrations. As described in the main text, both spectra were fit using the Drude dielectric function (Equation 4, main text). The resulting fit to the absorption profile measured for $Sn:In_2O_3$ NCs appears in Figure 1A of the main text, while the corresponding fit to WO_{3-x} NCs is displayed in Figure S2B below.

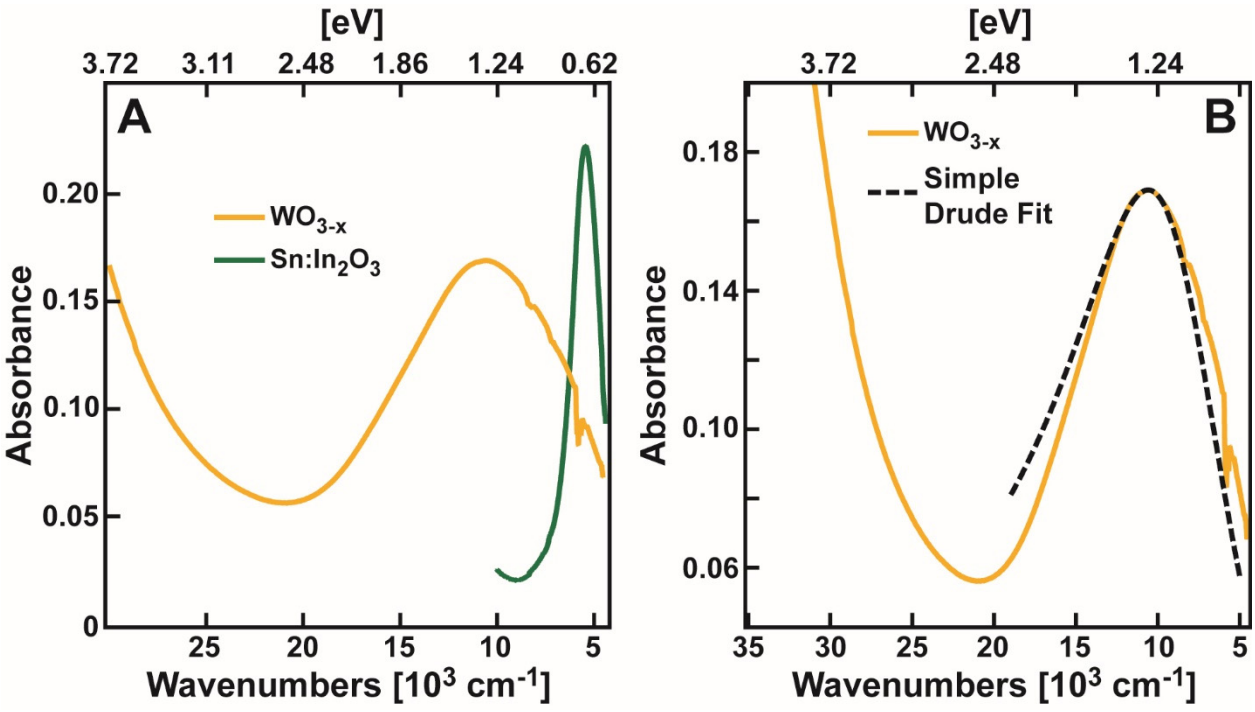

Figure S2: (A) Absorption spectra of WO_{3-x} and $Sn:In_2O_3$ NCs used for TA experiments. (B) Drude fit (black dashed) to the WO_{3-x} NC absorption spectrum (yellow) used extract dielectric constants needed for calculating thermal properties.

Extraction of the Electron-phonon Coupling Constant, G

Figures 4A and 4B of the main text display TA decay curves that highlight the loss of photobleaching signal produced for both $Sn:In_2O_3$ and WO_{3-x} NCs following photoexcitation. As outlined in the main text, these curves display two characteristic timescales, a sub-picosecond decay due to equilibration between hot electrons and lattice phonons, and a much longer decay that unfolds over hundreds of picoseconds and reflects the dissipation of energy from excited phonons to the solvent surrounding each NC. As the excitation fluence is increased in $Sn:In_2O_3$ NCs, there is a notable slowing of the electron-phonon equilibration timescale that results from the increased initial electron temperature imparted to each NC by the pump pulse. An exponential decay was fit to the decay traces measured data for $Sn:In_2O_3$ NCs between 0.15 and 1.5 ps while a fit to the WO_{3-x} decay traces was performed between 0.20 and 1.5 ps. The recovered decay rate was taken to be a good approximation of the electron relaxation timescale and its variation with excitation fluence is shown in Figure S3A. The electron-phonon coupling constant, G, for $Sn:In_2O_3$ NCs

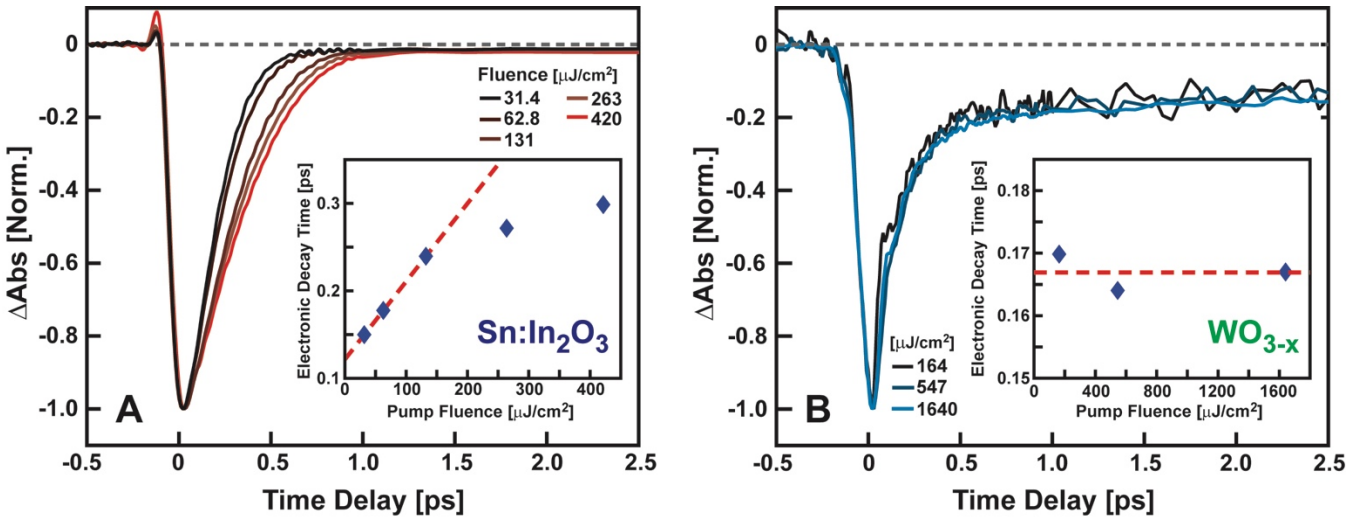

Figure S3: TA decay curves data shown in Figures 4A for ($Sn:In_2O_3$, panel A) and 4B (WO_{3-x}, panel B) of the main text, but normalized to highlight changes in the electron cooling rate with excitation fluence. The inset of each panel plots the characteristic timescale extracted from each curve from a single exponential fit. For $Sn:In_2O_3$, a linear fit to the low pump fluence data was used to determine τ_0. Higher fluence points were excluded due to nonlinearity of the NCs' LSPR at sufficiently high electron temperature.[1] For WO_{3-x}, no dependence of the electron cooling rate was observed for the fluences investigated. As such, the average decay rate recovered from the data was used to determine τ_0.

can be extracted from this data by extrapolating changes in the electronic decay rate to zero excitation fluence to determine the limiting electron-phonon equilibration rate at room temperature,[1]

$$G = \frac{\gamma T_0}{\tau_0}. \quad \text{(S1)}$$

In the above equation, τ_0 represents the extrapolated electronic decay time at zero pump fluence, T_0 represents the temperature of the NC's surroundings (taken to be 298 K), and γT_0 is the electron heat capacity of the NC at its starting temperature. Extrapolating the recovered fits to zero fluence gives a τ_0 value of 122 fs, which together with the reported value for γ for $Sn:In_2O_3$ NCs (Table 2, main text) yields $G = 1.25 \times 10^{10}$ J/K•s•cm^{-3}.

In contrast, increasing the excitation fluence over a comparable range as that used to excite $Sn:In_2O_3$ NCs had no measurable impact on the electron-phonon equilibration rate for WO_{3-x} NCs, as illustrated in Figure S3B. This likely reflects the larger value of γ for WO_{3-x} with respect to $Sn:In_2O_3$, which prevents the electronic temperature of WO_{3-x} NCs from appreciably heating at the excitation densities used. As

such, the average decay rate measured across our data sets as a measure of the electron-phonon equilibration rate, τ_0, for WO_{3-x} NCs was found to be 167 fs. Combining this with WO_{3-x}'s γ value (Table 2, main text) gives G = 9.64 × 10^{10} J/K•s•cm^{-3}. Based on error associated with fitting the Sn:In_2O_3 and WO_{3-x} decay curves, we estimate the error in these extracted G values as roughly ±5%.

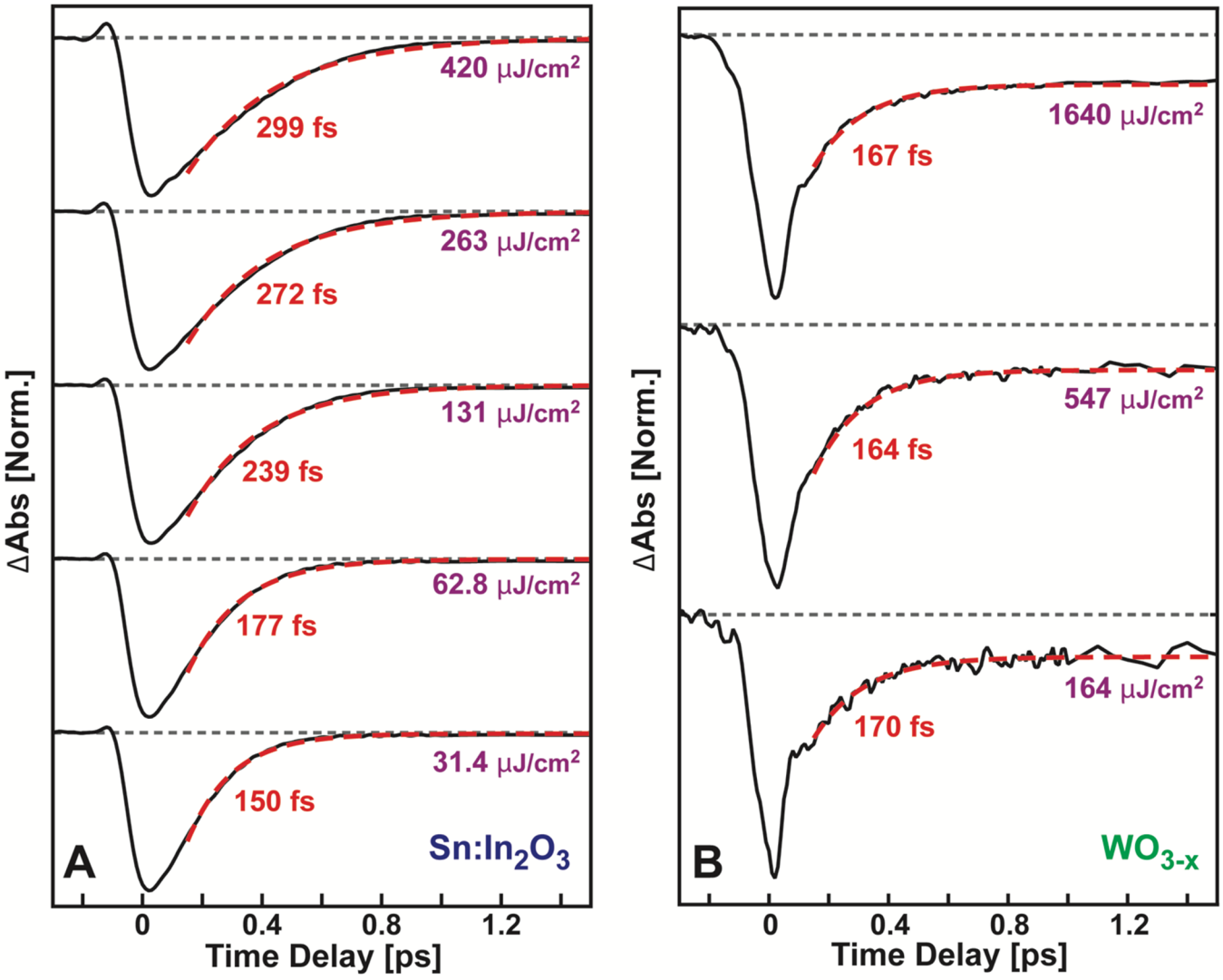

Figure S4: TA decay curves data shown in Figures S3 for Sn:In_2O_3 and WO_{3-x}, with exponential fits included for extracting the lifetime of the hot electron equilibration with the lattice.

Phonon-Bath Equilibration of Metal Oxide Nanocrystals

Following LSPR excitation of a colloidal NC, hot electrons transfer their energy to lattice phonons that in turn release their energy to their surroundings. While the focus of this manuscript has been on the

equilibration of hot electrons and lattice phonons, which occurs in metal oxide NCs on sub-picosecond timescales, our measured TA spectra also display kinetics that unfold over tens-to-hundreds of picoseconds that can largely be ascribed to lattice relaxation. Figure S4 replots the same decay curves shown in Figures 4A and 4B of the main text, but on an expanded time axis. While the majority of the photobleach recovery shown for Sn:In_2O_3 NCs (Figure S4A) and WO_{3-x} NCs (Figure S4B) is complete within less than one picosecond, a persistent photobleach can be seen for each sample that persists over hundreds of picoseconds (Figure S5). Heating of a NC's lattice is expected to lead to a broadening of its LSPR, which in TA measurements will lead to a photobleaching signal near the peak of the NC's LSPR. As the excitation fluence is increased, we observe that the magnitude of the photobleaching signal increases, as would be expected if these changes reflected the temperature of the NC lattice. TA spectra measured out to time delays of ~1.7 ns show that this signal relaxes towards baseline, but the rate with which they do depends on NC size. Given that the focus of our manuscript is on electron-phonon equilibration, we leave a detailed description of phonon relaxation to future work.

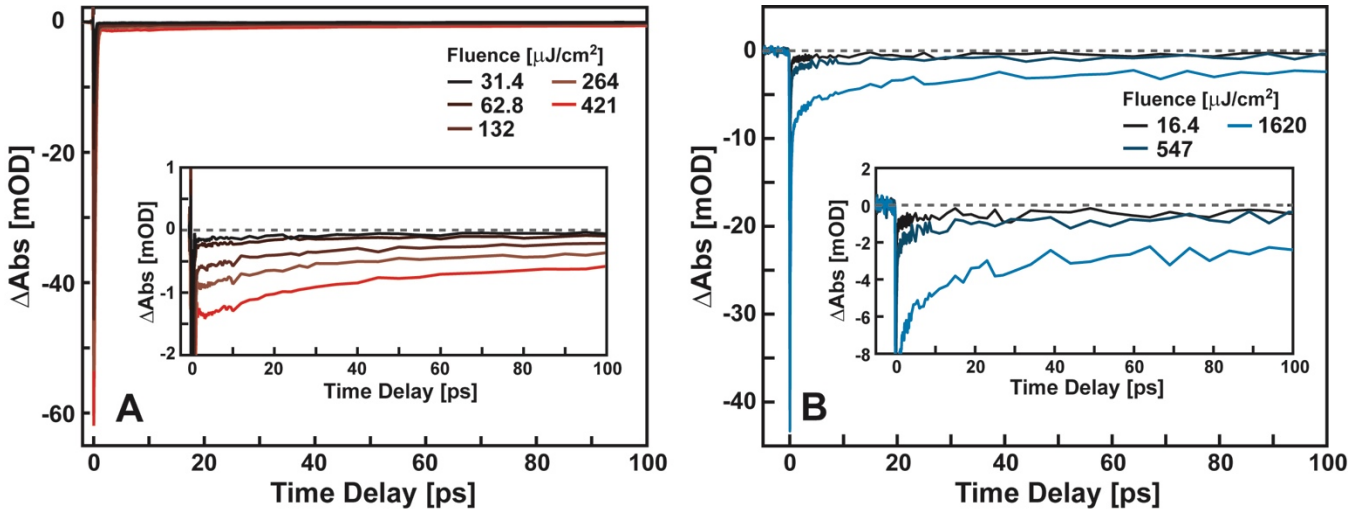

Figure S5: Reproduction of the TA decay curves for Sn:In_2O_3 NCs (A) and WO_{3-x} NCs (B) shown in Figure 4 of the main text, but over an expanded time range. (Inset) Zoomed in plot of each set of data showing a persistent photobleaching signal that can be ascribed to lattice heating.

Expected Transient Absorption Lineshapes for Two-temperature Model Relaxation

As briefly described in the main text, the presence of hot electrons and excited lattice phonons will both give rise to spectral changes in the absorption lineshape of a NC's LSPR that can be observed by TA spectroscopy.[2] Specifically, the presence of hot electrons will lead to an increase in a NC's high frequency dielectric constant, ε_∞, which induces a bathochromic shift of the NC's LSPR. Likewise, increasing a NC's lattice temperature will induce a broadening of its LSPR due to an increase in the LSPR's damping coefficient, Γ. Figure S6 shows a model calculation of TA lineshapes that are expected to result from these two different processes over the range currently accessible by our InGaAs array detector for a LSPR centered at 1830 nm, which limits us to only viewing changes that occur to the high frequency side of the LSPR. Spectra shifting due to electronic heating leads to a negative photobleaching signal across our entire spectral range (Figure S6, black curve) while LSPR broadening due to lattice heating gives rise to the appearance of a positive signal near the high and low frequency edges of the LSPR (Figure S6, green curve). These changes are qualitatively consistent with TA spectra measured at short (~250 fs) and long time delays (~5 ps) for Sn:In_2O_3 NCs (main text, Figure 4C).

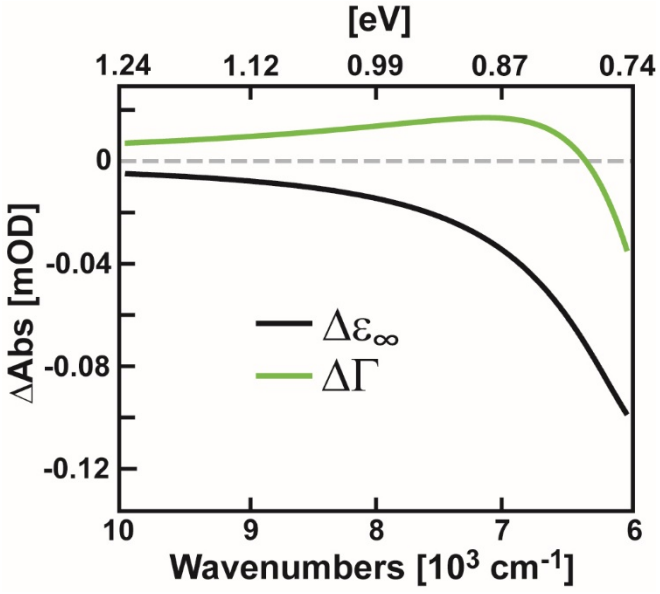

Figure S6: Expected TA signals using our dielectric function for Sn:In_2O_3. Electronic heating of the NC results in a shift of the LSPR to lower energy due to an increase in ε_∞, which results in a negative photobleaching signal on the high-energy side of the LSPR (black). Phonon excitation of the NC leads to a broadening of the LSPR due to a decrease in its damping coefficient, Γ, and hence the appearance of an induced absorption signal on the LSPR's high frequency side (green).

References

(1) Hodak, J. H.; Martini, I.; Hartland, G. V. Spectroscopy and Dynamics of Nanometer-Sized Noble Metal Particles. *J. Phys. Chem. B* **1998**, *102* (36), 6958–6967.

(2) Scotognella, F.; Della Valle, G.; Srimath Kandada, A. R.; Dorfs, D.; Zavelani-Rossi, M.; Conforti, M.; Miszta, K.; Comin, A.; Korobchevskaya, K.; Lanzani, G.; et al. Plasmon Dynamics in Colloidal $Cu_{2-x}Se$ Nanocrystals. *Nano Lett.* **2011**, *11* (11), 4711–4717.